Suppression of Antifolate Resistance by Targeting the Myosin Va Trafficking Pathway in Melanoma[1,2]

María Piedad Fernández-Pérez[*,3],
María F. Montenegro[*,3], Magalí Sáez-Ayala[*],
Luis Sánchez-del-Campo[*,4],
Antonio Piñero-Madrona[†], Juan Cabezas-Herrera[‡]
and José Neptuno Rodríguez-López[*]

[*]Department of Biochemistry and Molecular Biology A, School of Biology, Regional Campus of International Excellence "Campus Mare Nostrum", University of Murcia, Murcia, Spain; [†]Department of Surgery, University Hospital Virgen de la Arrixaca, Instituto Murciano de Investigación Biosanitaria, Murcia, Spain; [‡]Translational Cancer Research Group, University Hospital Virgen de la Arrixaca, Instituto Murciano de Investigación Biosanitaria, Murcia, Spain

Abstract

Human melanoma is a significant clinical problem. As most melanoma patients relapse with lethal drug-resistant disease, understanding and preventing mechanism(s) of resistance is one of the highest priorities to improve melanoma therapy. Melanosomal sequestration and the cellular exportation of cytotoxic drugs have been proposed to be important melanoma-specific mechanisms that contribute to multidrug resistance in melanoma. Concretely, we found that treatment of melanoma with methotrexate (MTX) altered melanogenesis and accelerated the exportation of melanosomes; however, the cellular and molecular processes by which MTX is trapped into melanosomes and exported out of cells have not been elucidated. In this study, we identified myosin Va (MyoVa) as a possible mediator of these cellular processes. The results demonstrated that melanoma treatment with MTX leads to Akt2-dependent MyoVa phosphorylation, which enhances its ability to interact with melanosomes and accelerates their exportation. To understand the mechanism(s) by which MTX activates Akt2, we examined the effects of this drug on the activity of protein phosphatase 2A, an Akt inhibitor activated by the methylation of its catalytic subunit. Taken together, this study identified a novel trafficking pathway in melanoma that promotes tumor resistance through Akt2/MyoVa activation. Because of these findings, we explored several MTX combination therapies to increase the susceptibility of melanoma to this drug. By avoiding MTX exportation, we observed that the E2F1 apoptotic pathway is functional in melanoma, and its induction activates p73 and apoptosis protease-activating factor 1 following a p53-autonomous proapoptotic signaling event.

Neoplasia (2013) 15, 826–839

Introduction

During the past 30 years, the incidence and annual mortality of melanoma has increased more rapidly than any other cancer, and according to an American Cancer Society estimate, there were approximately 76,250 new invasive melanoma cases diagnosed in 2012 in the United States, which resulted in approximately 9180 deaths [1]. Unfortunately, this increase in incidence has not been paralleled by the development of new therapeutic agents with a significant impact on survival and metastatic melanoma is still an incurable disease. Although many patients with melanoma localized to the skin are cured by surgical excision, other patients with advanced disease who have lymph node involvement or distant metastases have 5-year survival rates of 50% and 10% to 20%, respectively [2]; this poor prognosis largely results from melanoma resistance to conventional chemotherapy [3–8]. In this context, the identification of novel pathways in melanoma, susceptible of drug targeting, might help to develop novel therapies and drug combinations to improve treatment efficacy and avoid drug resistance in this malignant pathology.

Accumulating evidence has indicated that melanosomes contribute to the refractory properties of melanoma cells by sequestering cytotoxic drugs and increasing melanosome-mediated drug export [4–7]. On the basis of these observations, it has been suggested that preventing melanosomal sequestration of cytotoxic drugs, by inhibiting the functions of melanosomes, may have great potential as an approach to improving the chemosensitivity of melanomas [4]. Recently, several mutational and RNA interfering approaches have identified novel protein-trafficking molecules involved in melanoma resistance; melanoma cells depleted of genes such as *gp100/Pmel17*, *Dtnbp1*, *Pldn*, *Vps33a*, or *Hps6*, which participate in biogenesis or trafficking of melanosomes, showed increased sensitivity to cisplatin and other cytotoxic drugs [6,7]. However, despite the great advances in the knowledge of this multidrug resistance mechanism, the processes by which drugs are trapped into melanosomes and exported out of cells remains largely undetermined and the existence of drug-based therapies, to suppress this mechanism of resistance, is still limited.

To identify novel druggable targets into this multidrug resistance mechanism, we evaluated the resistance of melanoma to methotrexate (MTX), a drug in widespread clinical use but is not actively used for melanoma treatment [9]. As for other drugs, we have recently observed that the folate receptor α–mediated endocytotic transport of MTX facilitates melanosomal drug sequestration and cellular exportation in melanoma cells, thereby reducing the accumulation of MTX in intracellular compartments [5]. Therefore, to achieve our objective, we focused our attention on the MTX effects on myosin Va (MyoVa), an actin-based motor protein involved in vesicle trafficking during exocytosis [10]. We observed that the MyoVa protein was specifically phosphorylated in response to MTX treatment, stimulating MyoVa-dependent melanosome transport. Therefore, once we elucidated the molecular mechanisms leading to MTX-dependent MyoVa activation in melanoma, we tested whether pharmacologic blockade of the MyoVa pathway could overcome MTX resistance in these cells. Because melanoma cells are intrinsically resistant to classic antifolates [11], the death pathways triggered in melanomas in response to this class of drugs have never been studied. Therefore, in addition to its clinical potential, this study allowed us to analyze, for the first time, the melanoma susceptibility to classic antifolates and identify functional apoptosis pathways in this evasive and deadly cutaneous pathology.

Materials and Methods

Reagents and Antibodies

MTX, 7-hydroxystaurosporine (UCN-01), cantharidin, and Akt inhibitor (IAKT) VIII trifluoroacetate salt hydrate were obtained from Sigma-Aldrich (Madrid, Spain). Antibodies against the following proteins were used: Akt1, Akt2, phospho-Akt1/2/3-Thr^{308}, phospho-Akt1/2/3-Ser^{473}, phospho-H2A.X-Ser^{139}, E2F1, p73, protein phosphatase 2A C (PP2A C) subunit, methyl–PP2A C subunit (Millipore, Madrid, Spain), Akt3, Akt1/2/3, Melan-A/MART1, p53, Slac2-a (Santa Cruz Biotechnology, Santa Cruz, CA), MyoVa (Cell Signaling Technology, Danvers, MA), apoptosis protease-activating factor 1 (Apaf1; BD Biosciences, Sparks, MD), Pmel17/HMB45 (Dako Inc, Carpinteria, CA), Rab27a (Abcam, Cambridge, United Kingdom), and β-actin (Sigma).

Cell Lines, Proliferation, and Apoptosis Assays

Melanoma cell lines of human and mouse origin were obtained from ATCC (Manassas, VA) and maintained in the appropriate culture medium supplemented with 10% FBS and antibiotics. Cell viability was evaluated using 3-(4,5-dimethylthiazol-2-yl)-2,5-diphenyl-tetrazolium bromide. Cells were evaluated for apoptosis using the Cell Death Detection ELISA^{PLUS} Kit (Roche Diagnostics, Barcelona, Spain) that detects mononucleosomes and oligonucleosomes in the cytoplasmic fractions of cell lysates using biotinylated anti-histone and peroxidase-coupled anti-DNA antibodies. The amount of nucleosomes is spectrophotometrically quantified at 405 nm by the peroxidase activity retained in the immunocomplexes. Apoptosis was defined as the specific enrichment of mononucleosomes and oligonucleosomes in the cytoplasm and was calculated by dividing the absorbance of treated samples by the absorbance of untreated samples after correcting for the number of cells. The induction of apoptosis in each melanoma cell line after a 7-hour treatment with 2 μM staurosporine (100% apoptotic cells) was used to calculate the number of apoptotic cells.

Polymerase Chain Reaction Analysis

mRNA extraction, cDNA synthesis, and conventional and quantitative real-time polymerase chain reaction (PCR) were performed as previously described [12]. Primers were designed using Primer Express version 2.0 software (Applied Biosystems, Foster City, CA) and synthesized by Life Technologies (Barcelona, Spain). To quantify the gene expression level of the MyoVa exon F transcripts, the following primers were designed for exons E and F [Accession Nos AF090424 and X57377 for human (h) and mouse (m) transcripts, respectively]: *MyoVa* (h) (forward: 5′-GGC TGA CCA ACG AAA ACT TG-3′ and reverse: 5′-TCA TCC GTT TGT AAA GGG AAA T-3′) and *MyoVa* (m) (forward: 5′-GGC TGA CCA ATG AAA ACC TG-3′ and reverse: 5′-TCC TTT TGT AAA GTG AAA TCC GAT A-3′). p73 primers were designed to amplify TAp73 (p73 with the transactivating domain; NM_005427.3) transcripts of human origin: *TAp73* (h) (forward: 5′-TGG AAC CAG ACA GCA CCT ACT TCG-3′ and reverse: 5′-CAG GTG GCT GAC TTG GCC GTG CTG-3′). Other primers included are given as follows: *Apaf1* (h) (forward: 5′-GCT CTC CAA ATT GAA AGG TGA AC-3′ and reverse: 5′-ACT GAA ACC CAA TGC ACT CC-3′) and *β-actin* (h, m) (forward: 5′-AGA AAA TCT GGC ACC ACA CC-3′ and reverse: 5′-GGG GTG TTG AAG GTC TCA AA-3′).

Chromatin Immunoprecipitation Assays

A chromatin immunoprecipitation (ChIP) assay was performed using the Magna ChIP G Kit from Millipore according to the manufacturer's instructions. Briefly, untreated and MTX- and/or UCN-01–treated SK-MEL-28 cells were formaldehyde cross-linked, and the DNA was sheared by sonication to generate an average size of 300 to 3000 bp. The chromatin was then incubated with anti-E2F1 or mouse IgG antibodies. DNA from lysates before immunoprecipitation was used as a positive input control. After washing, elution, and DNA purification, the DNA solution (2 μl) was used as a template for quantitative real-time PCR amplification using specific human primers. The following primer sequences were used for ChIP-PCR: *TAp73* promoter region (forward: 5′-TGA GCC ATG AAG ATG TGC GAG-3′ and reverse: 5′-GCT GCT TAT GGT CTG ATG CTT ATG-3′) and *glyceraldehyde 3-phosphate dehydrogenase* (*GAPDH*) (forward: 5′-CAA TTC CCC ATC TCA GTC GT-3′ and reverse: 5′-TAG TAG CCG GGC CCT ACT TT-3′). Standard curves were generated for all primer sets to confirm linearity of signals over the experimentally measured ranges.

Interference RNA

Specific stealth siRNAs for *MyoVa* (HSS106896), *p53* (HSS129934 and HSS129936), *Akt1* (HSS100345 and HSS100346), *Akt2* (HSS163235 and HSS163236), and *Akt3* (HSS115177 and HSS115179) were obtained from Life Technologies and transfected into melanoma cells using Lipofectamine 2000 (Life Technologies). Treatments began 24 hours after siRNA transfection. Stealth RNA negative control duplexes (Life Technologies) were used as control oligonucleotides, and the ability of the stealth RNA oligonucleotides to knock down the expression of the selected genes was analyzed by Western blot analysis 24 hours after siRNA transfection.

Immunoblot Analysis and Immunoprecipitation

Whole-cell lysates were collected by adding sodium dodecyl sulfate sample buffer. After extensive sonication, the samples were boiled for 10 minutes and subjected to sodium dodecyl sulfate–polyacrylamide gel electrophoresis. Proteins were then transferred to nitrocellulose membranes and analyzed by immunoblot analysis (ECL Plus; GE Healthcare, Barcelona, Spain). For Akt2 immunoprecipitation assays, the cells (approximately 5×10^6) were lysed in 500 μl of lysis buffer [50 mM Tris (pH 8.0), 300 mM NaCl, 0.4% NP-40, and 10 mM $MgCl_2$] supplemented with protease and phosphatase inhibitor cocktails (Sigma). Cell extracts were cleared by centrifugation ($20,000g$ for 15 minutes) and then diluted with 500 μl of dilution buffer [50 mM Tris (pH 8.0), 0.4% NP-40, and 2.5 mM $CaCl_2$] supplemented with protease and phosphatase inhibitor cocktails and DNase I (Sigma). Extracts were precleared by a 30-minute incubation with 20 μl of PureProteome Protein G Magnetic Beads (Millipore) at 4°C with rotation. An Akt2 antibody was then added to the precleared extracts. After incubation for 1 hour at 4°C, 50 μl of PureProteome Protein G Magnetic Beads was added, and the extracts were further incubated for 20 minutes at 4°C with rotation. After extensive washing, the bound proteins were analyzed by Western blot analysis. Unbound extracts were used as positive inputs for protein load determination.

Microscopy and Fluorescence Lifetime Imaging Microscopy

EM was performed as previously described [13] using a Zeiss EM10 electron microscope (Carl Zeiss MicroImaging, Inc, Thornwood, NY). Laser scanning confocal microscopy of fixed cells was performed using a Leica TCS 4D confocal microscope (Wetzlar, Germany). For indirect immunofluorescence studies, preparations of cells on glass slides were fixed with cold acetone for 5 minutes and washed with phosphate-buffered saline (PBS). The cells were incubated with 3% BSA for 20 minutes and then with primary antibodies (diluted 1:200 in PBS containing 1% BSA) for 2 hours at room temperature. The cells were washed three times in PBS and incubated for 1 hour at room temperature with Alexa Fluor dyes (Life Technologies) as secondary antibodies. After three washes with PBS, the cells were incubated with 0.01% 4′-6-diamidino-2-phenylidene (DAPI; Sigma) in water for 5 minutes. For antibody specificity, primary antibodies were replaced with specific IgGs (diluted 1:200) during immunofluorescence. Co-localization analysis was performed with the Co-localization Finder plugin of ImageJ-NIH and showed images of the Alexa Fluor 633 (red) merged with Alexa Fluor 488 (green) secondary antibodies and the co-localized pixels in orange. This plugin provides the Pearson overlap coefficient (*Rr*) ranging from –1 to 1, where 1 represents perfect co-localization, 0 represents random co-localization, and –1 represents perfect exclusion (http://rsb.info.nih.gov/ij/plugins/colocalization-finder.html).

The confocal imaging of MTX–fluorescein isothiocyanate (FITC) in live cells [fluorescence lifetime imaging microscopy (FLIM)] was performed using the same confocal microscope. Images were collected following 488-nm laser excitation with an FITC emission filter. Before live confocal microscopy, the cells were incubated in serum-free Dulbecco's modified Eagle's medium (DMEM) for 1 hour with MTX-FITC and with or without UCN-01. After this time, the cells were extensively washed with DMEM containing MTX (without FITC) and with or without UCN-01 as appropriate. During imaging, the cells were incubated on a heated stage at 37°C in DMEM containing MTX (without FITC) and with or without UCN-01 as appropriate. Frames were collected at the indicated times. Images were processed with Huygens Essential v. 4.1.0p6 (Scientific Volume Imaging BV, Hilversum, The Netherlands) and Imaris (Bitplane AG, Zurich, Switzerland). Vesicle movements were traced, and velocities and distances were calculated using the ImageJ 1.6.0_20 (National Institutes of Health, Bethesda, MD) manual tracking plugin (Fabrice Cordelieres, Institut Curie, Orsay, France). The fluorescence intensity levels within selected cell areas were also computed using ImageJ, and the FITC fluorescence intensity was expressed as integrated density (reactive area multiplied by the mean gray of the same area).

Preparation of Melanoma Cell Granular Fractions and Sucrose Density Gradients

Control untreated melanoma cells and those subjected to treatments with MTX and/or IAKT were harvested with a mixture of 0.25% trypsin and 0.25 mM EDTA, washed once in 0.25 M sucrose, and centrifuged at $1000g$ for 10 minutes at 4°C. Specimens were then homogenized on ice using 20 strokes in a Potter homogenizer and centrifuged at $1000g$ for 10 minutes at 4°C. The supernatant was recovered and further centrifuged at $19,000g$ for 30 minutes at 4°C [14]. The pellet containing melanosome-enriched granular fractions was resuspended in ice-cold 0.25 M sucrose in 10 mM Hepes (pH 7.0) and examined by EM. Purified melanoma granular fractions were resuspended in 2.0 M sucrose and layered at the bottom of a 1.0 to 2.0 M sucrose step (1.0, 1.2, 1.4, 1.5, 1.6, 1.8, and 2.0 M) gradient. The gradient was centrifuged at $100,000g$ in a Beckman SW 41 swinging bucket rotor for 1 hour at 4°C.

PP2A Assay

Cells were exposed to the experimental conditions indicated in the results. After two washes with 0.9% NaCl, total cellular proteins were extracted in lysis buffer containing 50 mM Tris·HCl (pH 7.5), 250 mM NaCl, 3 mM EDTA, 3 mM EGTA, 1% Triton X-100, and 0.5% NP-40 without phosphatase inhibitors. Specific PP2A activity was measured using the PP2A Immunoprecipitation Phosphatase Assay Kit (Millipore). All procedures were performed according to the manufacturer's protocol, and changes in absorbance were measured at 650 nm in a Spectra-MAX 250 (Molecular Devices, Sunnyvale, CA) plate reader.

MTX Conjugation with HRP

MTX (10 mM) was dissolved completely in a pH 7.0 buffer solution (100 mM, phosphate buffer), and then an equimolar quantity of N-(3-dimethylaminopropyl)-N′-ethylcarbodiimide hydrochloride (EDC; 10 mM) was added. The mixture was stirred for 40 minutes at room temperature. The activated MTX (1 ml) was added to 10 µM horseradish peroxidase isozyme C (HRPC) solutions (1 ml, pH 7.0) and incubated for 18 hours at room temperature. The MTX-conjugated proteins were separated from unreacted MTX using a Sephadex G-25 desalting column equilibrated in PBS (pH 7.4). The degree of MTX conjugation was spectrophotometrically determined by measuring the difference in absorbance between the conjugated and free proteins at 303 nm. HRP has a molecular mass of 40 kDa, and each HRP molecule contains six lysine residues. Titration experiments demonstrated that the total protein lysines were conjugated to MTX and this factor was used to determine MTX levels in melanoma cells (Figure 4*F*). The cellular uptake of MTX-conjugated HRP was performed by treating SK-MEL-28 melanoma cells (in 96-well plates) for 5 hours with 1 µM MTX-HRPC in the absence or presence of 50 nM UCN-01. After extensive washing with ice-cold PBS, the cells were disrupted by adding 200 µl of HRP activity medium [150 µM 2,2′-azino-bis(3-ethylbenzothiazoline-6-sulphonic acid) (ABTS) and 75 µM H_2O_2 in citrate-phosphate buffer, pH 4.5]. The oxidation of ABTS in the presence of HRP was followed by observing the increase in absorbance at 414 nm ($\Delta\varepsilon 414$ nm = 31.1 mM^{-1} cm^{-1}) in a SpectraMax 340PC384 microplate reader (Molecular Devices).

dNTP Pool Extraction and Analysis

Asynchronously proliferating SK-MEL-28 cells were seeded in six-well dishes. The extraction and analysis of the dNTP pools in each extract were performed as previously described [15]. The reaction mixtures (50 µl) contained 100 mM Hepes buffer (pH 7.5), 10 mM $MgCl_2$, 0.1 unit of the *Escherichia coli* DNA polymerase I Klenow fragment (Sigma, Madrid, Spain), 0.25 µM oligonucleotide template, and 1 µCi [³H]dATP (ARC, St Louis, MO) or [³H]dTTP (Perkin-Elmer, Waltham, MA). Incubations were performed for 60 minutes at 37°C.

Matrix-Assisted Laser Desorption/Ionization-Time-Of-Flight (MALDI-TOF) Mass Spectroscopy

SK-MEL-28 whole-cell lysates were immunoprecipitated as described above. After immunoprecipitation and elution, bound proteins were digested with trypsin according to standard procedures [16]. The data were recorded and processed with Agilent MassHunter Workstation Software to obtain the peptide mass fingerprint. The resulting peptide mass fingerprint mass spectra were searched against the MyoVa protein sequence with carbamidomethylation of cysteine as a fixed modification, and variable phosphorylation modifications at Ser[1650] and Ser[1812] were searched. The peptide mass tolerance was set to 50 ppm, and a maximum of three missed cleavages was considered.

Mouse Melanoma Models

Animals were bred and maintained according to the Spanish legislation on the "Protection of Animals Used for Experimental and Other Scientific Purposes" and in accordance with the directives of the European community. For the subcutaneous melanoma model, B16/F10 cells (5.0×10^5) were subcutaneously injected into the dorsal flanks of 6- to 8-week-old female C57BL/6 mice. Animals with tumors greater than 8 mm in diameter on day 8 or with no visible tumor growth by day 12 were excluded. Groups (*n* = 10 mice per group) were subjected to treatments beginning on the eighth day after tumor cell injection. Mice were intradermally treated with MTX (1 mg/kg per day) and/or UCN-01 (0.1 mg/kg per day) five times a week for 3 weeks.

Hepatic metastases were produced by the intrasplenic injection of 3.0×10^5 B16-F10-*luc2* mouse melanoma cells (Caliper Life Sciences, Hopkinton, MA) as previously described [17] (*n* = 10–15). Primary spleen tumors and hepatic metastases at days 12 and 14, respectively, were analyzed using the IVIS Imaging System (Caliper Life Sciences). Mice were intraperitoneally treated with MTX (1 mg/kg per day) and UCN-01 (0.5 mg/kg per day) from days 1 to 14, and control mice received the same volume of vehicle (DMSO). Postmortem histologic liver and spleen examination was performed in all animals. Formalin-fixed paraffin-embedded tissue sections were stained with hematoxylin and eosin. A Leica DMRB microscope connected to a Leica DC500 digital camera was used to quantify the number, average diameter, and position coordinates of the metastases [17]. For tyrosinase detection, mouse livers (three per treatment) were cut into approximately 0.2-g slices. Five randomly chosen slices from each liver were used for phenol-chloroform total RNA extraction. The RNA (5 µg) was then used to synthesize cDNA, and equal amounts of the five cDNA fractions corresponding with the same liver were pooled and employed for tyrosinase mRNA determinations using quantitative real-time PCR (tyrosinase primers—forward: 5′-GGG CCC AAA TTG TAC AGA GA-3′ and reverse: 5′-ATG GGT GTT GAC CCA TTG TT-3′).

Statistical Analysis

For experiments, the mean ± SD for five determinations in triplicate were calculated. Numeric data were analyzed for statistical significance using the Mann-Whitney *U* test for comparisons of mean values with the Statistical Package for the Social Sciences statistical software for Microsoft Windows, version 6.0 (Professional Statistic, Chicago, IL). Individual comparisons were analyzed with an unpaired two-tailed Student's *t* test. The criterion for significance was $P < .05$ for all comparisons.

Results

MTX Stimulates MyoVa-Dependent Melanosome Transport

The treatment of melanoma with MTX has been reported to accelerate melanosome exportation [5]. Here, we used FLIM to follow MTX-FITC–containing vesicles trafficking in SK-MEL-28 melanoma cells. Figure 1*A* demonstrates selected images from a typical experiment. Upon MTX-FITC addition, fluorescent vesicles migrated from the cytosol to the plasma membrane, and before being exported out of the
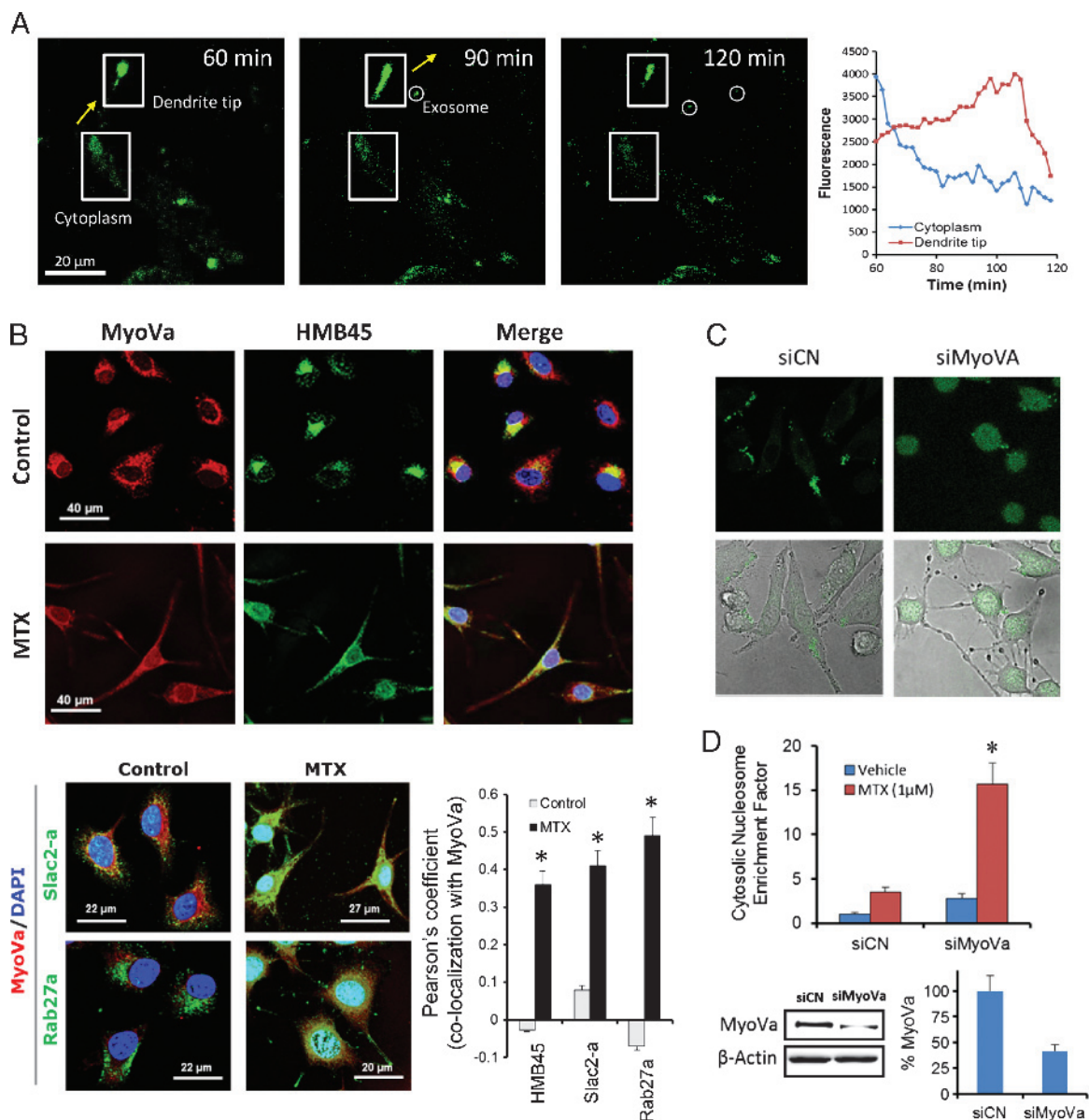
Figure 1. MTX activates MyoVa-dependent melanosome transport in melanoma. (A) Selected stills obtained by FLIM of MTX-FITC–containing vesicles in SK-MEL-28 cells treated with 20 μM MTX-FITC (1 hour). After extensive washing, the cells were imaged at one frame per minute for 1 hour in the presence of 20 μM unlabeled MTX. Time courses for the fluorescence intensity (arbitrary units) inside the boxed region of interest are shown. Fluorescent MTX-FITC–containing exosomes were visible during the recording time. (B) Immuno-histochemistry (IHC) was performed to analyze the localization of MyoVa in untreated SK-MEL-28 cells and in cells treated for 10 hours with 1 μM MTX. Upper panels show localization of MyoVa (red) and the melanosome stage II marker, HMB45 (green); DAPI is represented in blue. Lower panels represent merged images of the localization of MyoVa (red) and DAPI (blue) with Slac2-a or Rab27a (both in green). From the confocal images, a Pearson coefficient was calculated to estimate the degree of co-localization of the different melanosome markers with MyoVa (histograms). The Pearson overlap coefficients are represented as the average of 10 individual cells. *$P <$ .05 with respect to untreated control cells. (C) MyoVa silencing modifies MTX-FITC distribution in SK-MEL-28 melanoma cells. Cells were imaged after 1-hour treatment with 10 μM MTX-FITC. (D) MyoVa siRNA sensitizes SK-MEL-28 to MTX-induced toxicity. Upper panel: Apoptosis was determined after 72-hour treatments (*$P <$ .05 with respect to siControl (siCN)–treated cells; see Materials and Methods section). Lower panel: The effective silencing of MyoVa was tested by Western blot (WB) and relative to β-actin expression.

cells, they transiently accumulated in the dendritic tips of melanoma cells. It has been reported that melanosomes can be transported to melanocyte dendrites by the microtubule-based motor protein KIF3, and the subsequent movement of these vesicles and their tethering at the cell membrane is dependent on MyoVa and F-actin [18,19]. Because MTX-FITC treatment transiently increased fluorescent-containing vesicles in the actin-rich periphery of the dendrites, the effect of MTX

on the endogenous MyoVa localization in SK-MEL-28 was further analyzed by immunocytochemistry. Thus, an anti-MyoVa antibody was used in combination with the melanosomal marker HMB45 to analyze the distribution of melanosomes and their possible association with MyoVa in melanoma cells. As observed in Figure 1*B*, melanosomes were found perinuclear but did not co-localize with MyoVa in untreated cells (as determined by Pearson overlap coefficients); in contrast, after the

treatment of cells with MTX, MyoVa was localized in the cell periphery and the tips of the dendrites and associated with melanosomes. Co-localization studies of MyoVa with Rab27a and melanophilin/Slac2-a, two MyoVa-assistant proteins that contribute to melanosome transport [20,21], also suggested that MTX activated MyoVa-dependent mela-nosome transport in the amelanotic SK-MEL-28 melanoma cell line (Figure 1B). Activation of MyoVa-dependent melanosome transport by MTX was also confirmed in B16/F10, a highly melanotic murine cell line (Figure W1).

MyoVa Silencing Sensitizes Melanoma Cells to MTX-Induced Apoptosis

In melanocytes, MyoVa is required for the capture of melano-somes in actin-rich cell protrusions, and its specific silencing resulted in the dispersion of melanosomes in the cytoplasm [22]. Therefore, we next examined whether transient MyoVa silencing could sensitize melanoma cells to MTX by impeding its melanosome-mediated exportation (Figure 1C). SK-MEL-28 cells were transfected with siRNA-MyoVa or a control siRNA and maintained in culture medium in the presence or absence of MTX. The results presented in Figure 1D demonstrate that efficient MyoVa knockdown significantly increased the sensitivity of SK-MEL-28 cells to MTX-induced apoptosis.

MTX Leads to MyoVa Phosphorylation in Melanoma

Because MyoVa appeared to be an attractive target for avoiding MTX resistance in melanoma, we next sought to define the signaling pathways stimulated by MTX that result in the activation of MyoVa in these cells. First, we analyzed changes in the MyoVa expression levels after the treatment of melanoma cells with MTX. Real-time PCR and Western blot experiments indicated that MTX did not sig-nificantly increase the MyoVa mRNA and protein levels in these cells (Figure W2, A and B). Recent studies have provided evidence that the MyoVa protein is a direct Akt2 substrate in adipocytes. In addi-tion, Akt2-dependent MyoVa phosphorylation enhances its ability to interact with the actin cytoskeleton and GLUT4 vesicles [23]. There-fore, we next analyzed whether MTX treatment promoted MyoVa
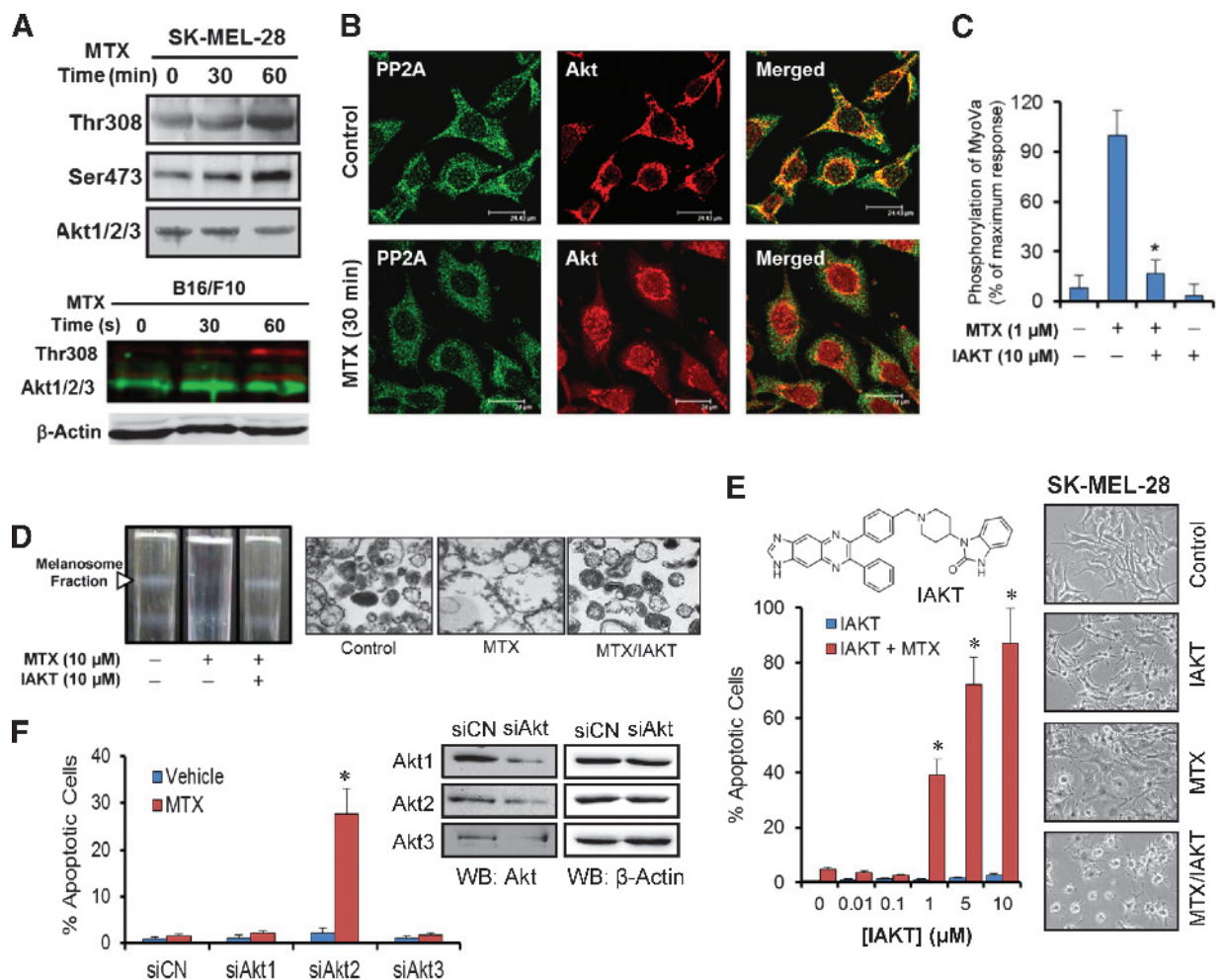
Figure 2. MTX activates the Akt-dependent phosphorylation of MyoVa in melanoma. (A) Effects of 1 μM MTX on Akt phosphorylation in melanoma cells. (B) IHC to analyze the location of Akt1/2/3 and PP2A in SK-MEL-28 (1 μM MTX). (C) Effect of IAKT (10 hours) on the MTX-induced phosphorylation of MyoVa (*$P < .05$). (D) Left panel: Density gradients of enriched melanosomal fractions obtained from untreated SK-MEL-28 cells and cells treated (5 hours) with 10 μM MTX and/or 10 μM IAKT. Right panel: EM experiments. (E) Histograms represent the effects of MTX/IAKT treatment (2 days) on SK-MEL-28 (*$P < .05$ with respect to IAKT-treated cells). Increasing IAKT con-centrations were analyzed in the absence or presence of 1 μM MTX. The images show the effects of MTX and/or IAKT treatments on cell morphology. (F) siCN- and siAkt-transfected cells were treated with 1 μM MTX (48 hours; *$P < .05$). Akt silencing was examined by WB.
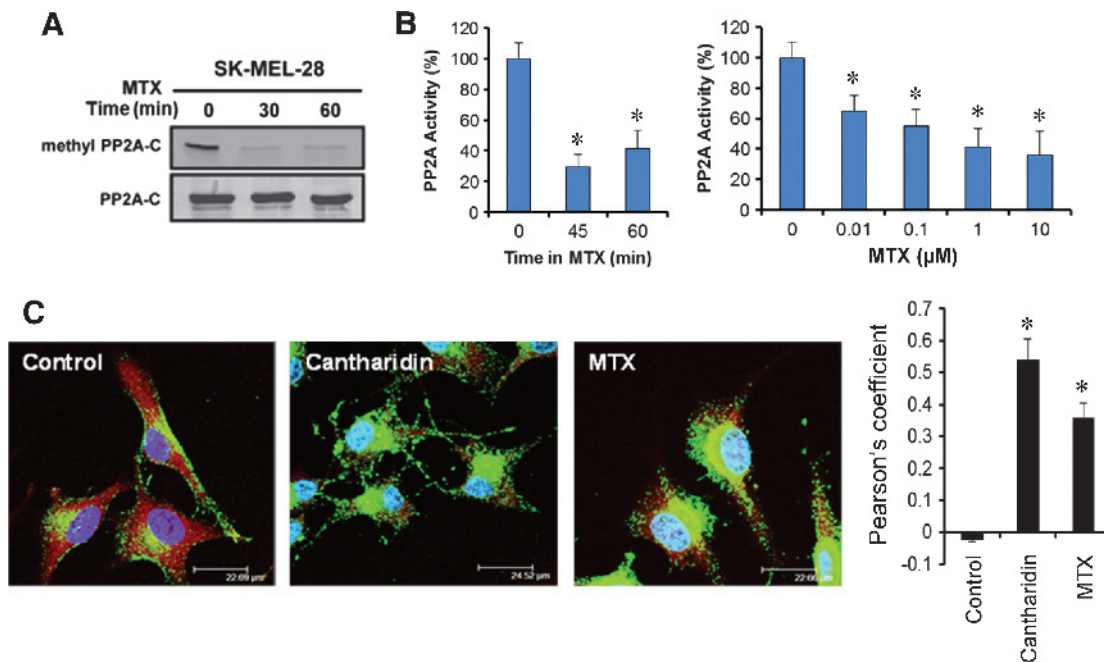
Figure 3. MTX induces demethylation of the catalytic PP2A C subunit and inhibits PP2A activity in melanoma cells. (A) Time-dependent effects of MTX (1 μM) on the methylation status of the catalytic PP2A C subunit (Leu[309]) in SK-MEL-28. (B) The histograms represent the time (at 1 μM MTX) and dose (at 60 minutes) effects of MTX on PP2A activity. *$P < .05$ compared with untreated controls. (C) Treatment of SK-MEL-28 melanoma cells during 24 hours with MTX or cantharidin (both at 1 μM) promoted the co-localization of MyoVa (red) with the melanosome stage II marker, HMB45 (green). DAPI is represented in blue. Merged images are shown. From the confocal images, a Pearson coefficient was calculated to estimate the degree of co-localization of MyoVa with HMB45 (histograms). The Pearson overlap coefficients are represented as the average of 10 individual cells. *$P < .05$ with respect to untreated control cells.

phosphorylation in melanoma. MyoVa has two Akt consensus motifs at Ser[1650] (RKRTSS) and Ser[1812] (RDRKDS), which are highly conserved across mammalian species. By using mass peptide analysis of immunoprecipitated MyoVa after trypsin digestion, we observed that MTX specifically promoted its phosphorylation at Ser[1650] (Figure W2C and Table W1).

MTX Activates Akt2-Dependent Phosphorylation of MyoVa in Melanoma

Western blot experiments indicated that MTX stimulates Akt phosphorylation at Thr[308] and Ser[473] in melanoma cell (Figure 2A). Akt activation by MTX was also confirmed with confocal microscopy experiments (Figure 2B), and it was found that activated Akt proteins translocated into the nucleus, coinciding with phosphorylation. MTX activation of the Akt-dependent phosphorylation of MyoVa in melanoma was also demonstrated by co-treatment of melanoma cells with MTX and a specific IAKT. The presence of IAKT during MTX treatments was sufficient to inhibit MyoVa phosphorylation and melanosome export (Figure 2, C and D), which resulted in a substantial increase in the sensitivity of melanoma cells to MTX-induced apoptosis (Figure 2E). Although the results indicated that MTX stimulated Akt phosphorylation, the identification of which Akt isoforms were activated by this drug in these experiments is difficult. Therefore, to identify which form of Akt may be involved in MyoVa activation in melanoma, we used siRNAs directed against the three Akt isoforms. For these experiments, SK-MEL-28 cells were transfected with these different siRNAs, and after 48 hours, the sensitivity of the transfected cells to MTX-induced apoptosis was determined. Each siRNA led to a marked depletion of the target protein (Figure 2F), but only the Akt2

knockdown significantly increased the sensitivity of the melanoma cells to MTX-induced apoptosis. In contrast, Akt1 and Akt3 knockdown had only marginal effects on MTX-induced apoptosis.

MTX Induces Demethylation of the Catalytic PP2A C Subunit and Inhibits PP2A Activity

In addition to nucleotide imbalance, a decrease in cellular methylation has been overlooked as a mechanism for the antiproliferative effects of MTX in cancer cells [24]. Because PP2A is now believed to dephosphorylate Akt at the Thr[308] phosphoinositide-dependent kinase-1 (PDK1) phosphorylation site, an attractive hypothesis that may link the MTX demethylating properties with Akt activation in melanoma is that MTX may inactivate PP2A, an IAKT activated by methylation of its catalytic subunit, before being exported from cells [25]. To test this hypothesis, we performed Western blot analysis, which demonstrated that MTX induced the demethylation of the PP2A on its catalytic subunit (Figure 3A). In agreement with this observation, MTX-dependent PP2A demethylation was also accompanied by a substantial time- and dose-dependent reduction in PP2A activity (Figure 3B) and a lack of its co-localization with Akt in the cytosolic compartment (Figure 2B). Next, we used cantharidin, a potent and selective inhibitor of PP2A, to confirm the consequences of PP2A inhibition on MyoVa activation in melanoma cells (Figure 3C).

UCN-01 Inhibits the MTX-Induced Activation of MyoVa and Prevents MTX Exportation in Melanoma Cells

Full Akt activation appears to require the phosphorylation of Thr[308] and Ser[473] by PDK1 and the putative PDK2, respectively. Because UCN-01 has been shown to potently inhibit PDK1 [26],

we hypothesized that the inhibition of Akt2 phosphorylation by UCN-01 may result in the disruption of MTX-stimulated melanosome transport. To validate this hypothesis, we examined the Akt2 phosphorylation state in total melanoma cell homogenates (Figure 4A). When cells were treated with UCN-01 in the presence of MTX, we observed a significant decrease in Akt2 phosphorylation (with respect to MTX-treated cells) at the Thr^{308} and Ser^{473} residues, which is consistent with PDK1 being the UCN-01 molecular target [26]. MALDI-TOF mass spectra of MyoVa tryptic peptides demonstrated that UCN-01–mediated Akt phosphorylation inhibition also resulted
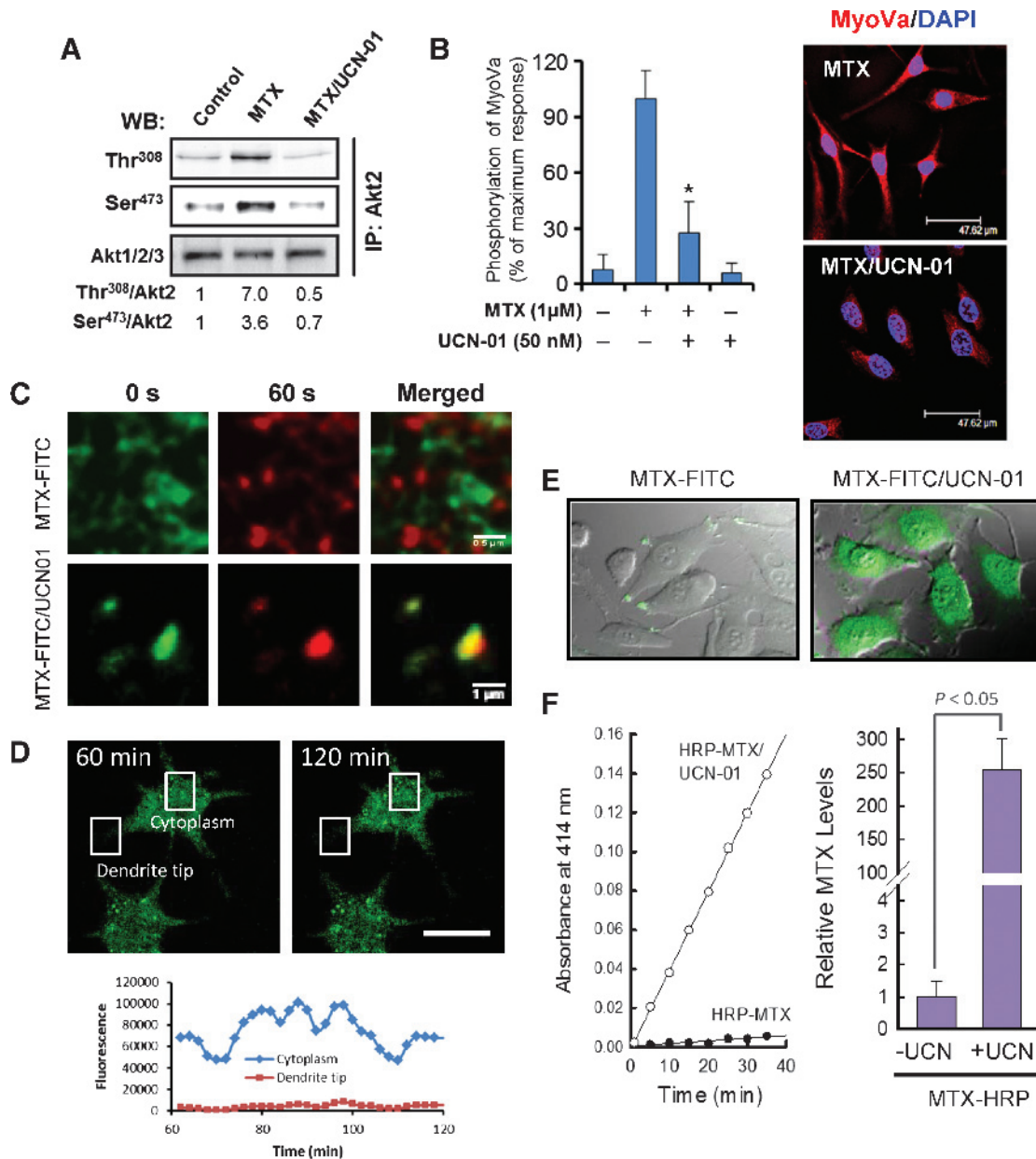
Figure 4. UCN-01 prevents MTX exportation in melanoma cells. (A) WB demonstrating the effects of UCN-01 on MTX-induced Akt2 phosphorylation. SK-MEL-28 cells were treated (1 hour) with 1 μM MTX or 1 μM MTX plus 50 nM UCN-01. (B) The effect of UCN-01 on the MTX-induced phosphorylation of MyoVa and its cellular localization. IHC was performed in SK-MEL-28 treated (10 hours) with 1 μM MTX or 1 μM MTX plus 50 nM UCN-01. (C) Subsecond frame-rate confocal microscopy examining the movements of individual MTX-FITC–containing vesicles. SK-MEL-28 cells were treated with 20 μM MTX-FITC or 20 μM MTX-FITC plus 50 nM UCN-01 for 1 hour. After extensive washing, the cells were imaged at two frames per second for 60 seconds in the presence of unlabeled MTX or MTX/UCN-01. Images at time zero are represented in green and those at 60 seconds are represented in red. (D) FLIM of MTX-FITC–containing vesicles in SK-MEL-28 treated with 20 μM MTX-FITC and 50 nM UCN-01 (1 hour). After extensive washing, the cells were imaged at one frame per minute for 1 hour in the presence of 20 μM unlabeled MTX and 50 nM UCN-01. Time courses of the fluorescence intensity inside the boxed regions of interest are shown. (E) Intracellular accumulation of MTX-FITC in SK-MEL-28 treated (4 hours) with MTX-FITC (20 μM) and MTX-FITC/UCN-01 (20 μM/50 nM). (F) HRP activity in SK-MEL-28 after treatment (4 hours) with MTX-HRP (1 μM) with and without UCN-01 (50 nM).
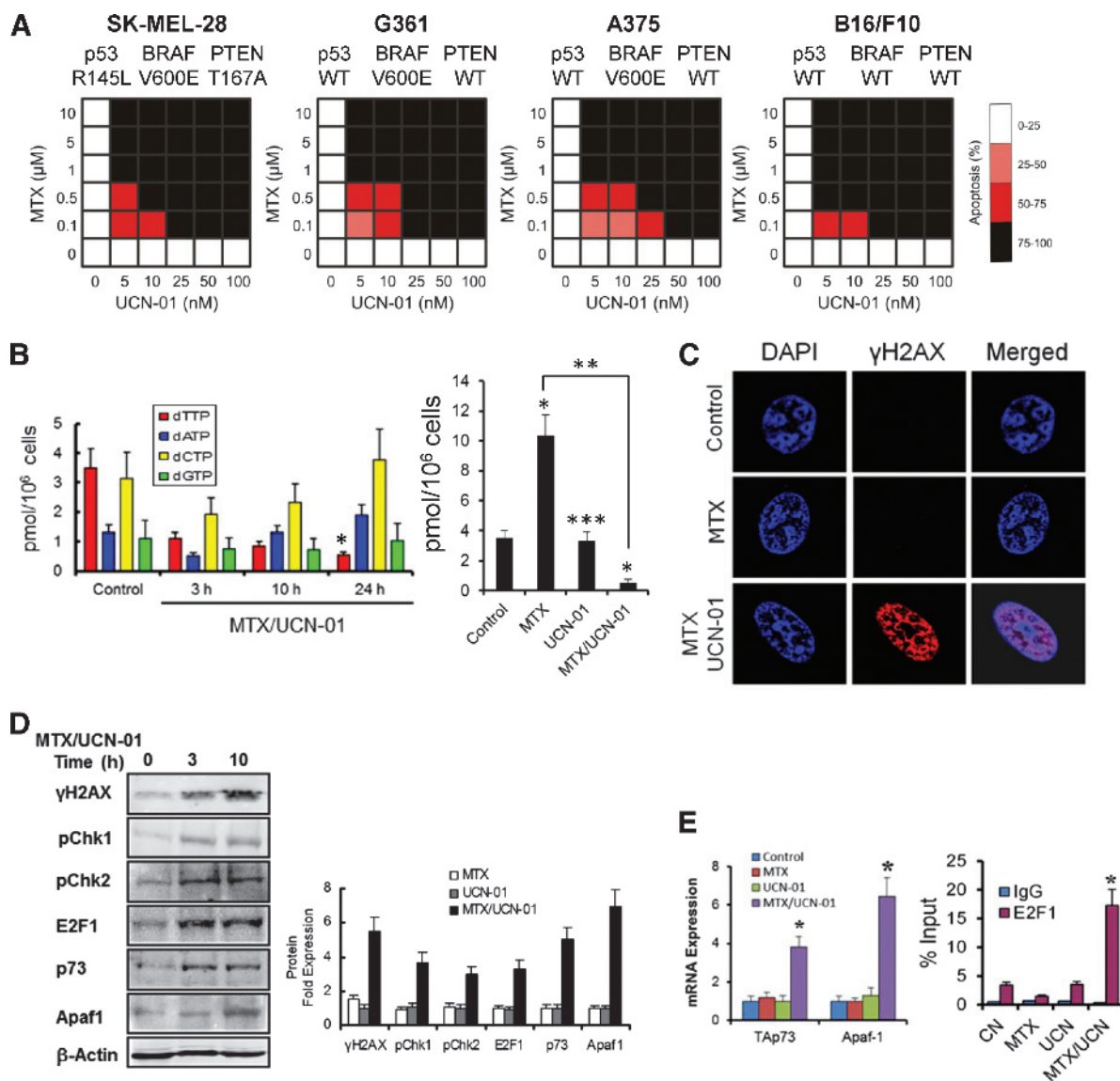
Figure 5. MTX/UCN-01 treatment induces E2F1-mediated apoptosis in melanoma. MTX (1 μM) and/or UCN-01 (50 nM) was used. (A) Synergy test for melanoma cell lines. MTX and UCN-01 were combined in 6×6 matrices where the concentration of one drug was increased along each axis. Apoptosis (4 days post-treatment) was obtained in triplicate in two-independent experiments. Differences in apoptosis in MTX/UCN-01–treated cells were significant with respect to individual treatments for each drug concentration ($P < .05$). MTX/UCN-01 combination showed clear synergistic behavior [45]. (B) dNTP quantification in melanoma cells. The data (left panel) were used to determine the total amount of each dNTP at each time point. The right panel represents dTTP levels in melanoma cells subjected to the indicated treatments (24 hours). *$P < .05$ with respect to untreated controls; **$P = .001$; ***not statistically significant with respect to the untreated controls. (C) SK-MEL-28 cells subjected to the indicated treatments (24 hours) were examined for γH2AX foci and DAPI. (D) WB of several melanocytic proteins after MTX/UCN-01 treatment (24 hours). Protein levels are relative to β-actin and the expression of these proteins in untreated controls (one-fold). (E) Left panel: Quantitative real-time PCR of TAp73 and Apaf1 mRNA. SK-MEL-28 cells were treated with the indicated treatments (24 hours). mRNA levels are presented relative to β-actin mRNA and compared with their expression levels in untreated cells (one-fold). Right panel: E2F1 occupancy on the TAp73 promoter of SK-MEL-28 subjected to the indicated treatments (24 hours).

in a significant reduction in the MTX-induced MyoVa phosphorylation at Ser[1650] (Figure 4B). Consequently, with this lack of MyoVa activation, we observed that UCN-01 prevented the MTX-mediated translocation of MyoVa to the melanoma dendritic tips (Figure 4B).

Given the remarkably dynamic nature of the MTX-FITC vesicle subpopulation observed in Figure 1A, we next used subsecond frame-rate confocal microscopy to examine the movement of individual MTX-FITC–containing vesicles in basal SK-MEL-28 cells

(Figure 4C). Fluorescent vesicles were observed to make directed movements over short distances at speeds ranging from 0.077 to 0.004 μm/s (average, 0.035 μm/s). However, in the presence of UCN-01, MTX-FITC vesicles remained fairly static over this time course, showing vibrational-type displacements but not moving far from their original location (Figure 4C). Because of this vesicle immobility, fluorescence was mainly associated with cytoplasmic compartments, and it did not migrate to the dendritic tips at longer time periods (Figure 4, D and E).

Finally, in an attempt to quantify the MTX accumulation in melanoma cells, we conjugated MTX to HRP, which served as a reporter enzyme (Figure 4F).

Suppression of MTX Exportation in Melanoma Cells Promotes E2F1-Mediated Apoptosis

Although UCN-01 exhibited potent antitumor activity in several *in vivo* and *in vitro* tumor models, this drug is inactive in melanomas [27]. However, when this drug was combined with MTX, we observed that apoptosis was strongly induced in melanoma cell lines independently of the mutational status of the *p53*, *BRAF*, and *PTEN* genes (Figure 5A). Although *p53* is usually wild type in melanoma, apoptosis triggered by MTX/UCN-01 treatment was independent of *p53* mutation status and was not affected by *p53* silencing in G361 cells (Figure W3). It is well known that antifolates induce dTTP depletion in sensitive cancer cells, and more recently, it has been proposed that "thymineless" death may be mediated by the E2F1 apoptotic cascade [28]. However, MTX fails to increase E2F1 protein levels in melanoma cells [9]. Because we previously hypothesized that this resistance mechanism was favored by low intracellular MTX levels in melanoma cells [5,9], we analyzed whether the higher MTX accumulation in the presence of UCN-01 could modify dTTP and E2F1 cellular levels. As observed in Figure 5, B and C, the treatment of melanoma cells with MTX/UCN-01 generated a nucleotide imbalance that favored dTTP depletion and the subsequent increase of E2F1 protein. Thymidine depletion induces DNA double-strand break (DSB) formation characterized by phosphorylation of histone H2AX at Ser^{139} (γH2AX) by ATM/ATR kinases and the subsequent rapid formation of γH2AX foci at the double-strand break sites [29]. Consistent with the effects of combination treatment being mediated through thymidine depletion, immunofluorescence revealed that combined MTX/UCN-01 treatment of SK-MEL-28 cells induced massive DNA damage in melanoma cells (Figure 5, C and D). In addition, Western blot and real-time PCR analyses (Figure 5, C and E) indicated that when combined with UCN-01, MTX induced the expression of both the transactivating form of p73 (TAp73) and Apaf1, two proapoptotic targets of E2F1 [30]. ChIP assays also indicated that, compared with untreated cells or those subjected to individual treatments, the MTX/UCN-01 combination significantly increased the occupancy of E2F1 at the *TAp73* promoter of SK-MEL-28 (Figure 5E). Because Chk1 and Chk2 are vital to E2F1 stabilization and activity after genotoxic stress, we next checked whether these checkpoint kinases were phosphorylated after MTX/UCN-01 treatment (Figure 5C). Altogether, these results indicated that the accumulation of MTX in cells co-treated with UCN-01 activated an E2F1-mediated but p53-independent cell death signaling in melanoma.

UCN-01 Enhances *In Vivo* Melanoma Sensitivity to MTX

The profound effects of this combination *in vitro* led us to test its antitumorigenic efficacy *in vivo*. In an initial approach, B16/F10 cells were subcutaneously injected into C57BL/6 mice, a syngeneic melanoma model in which host mice retain intact immune systems. Visual examination revealed that the MTX/UCN-01 combination acted synergistically to inhibit tumor growth (Figure 6A). Using B16 cells that express a luciferase reporter (Figure 6A), quantification of the *in vivo* luciferase signal confirmed that the MTX/UCN-01 combination was highly effective at reducing the primary tumor burden. A histologic study of primary splenic tumors suggested that MTX/UCN-01 treatment induced necrosis in B16/F10 tumors. As vehicle controls, B16/F10 tumors treated with DMSO showed their usual histologic appearance of poor differentiation and limited necrosis (Figure 6A). In contrast, 14-day treatment with MTX/UCN-01 induced obvious hemorrhagic necrosis, with necrotic areas of approximately 85%. Necrosis in splenic tumors was less evident in mice treated with MTX or UCN-01 (4 ± 2% and 2 ± 0.5%, respectively).

As an alternative approach, we tested whether MTX/UCN-01 administration after the injection of melanoma cells could prevent melanoma dissemination from the spleen to the liver, one of the preferential metastatic locations for melanomas. Luciferase-tagged B16/F10 cells were injected into the spleens of C57BL/6 mice, and after 14 days of treatment, the number of macroscopic liver metastases was assessed using a dissecting microscope (Figure 6B). Luciferase imaging demonstrated that mice treated with MTX/UCN-01 had an appreciably lower burden of macroscopic liver metastases compared with the untreated control (Figure 6B). To confirm the bioluminescent results, the livers were analyzed by histology at necropsy (Figure 6C). MTX/UCN-01 treatment reduced the hepatic metastasis volume by 50% compared with control mice treated with vehicle. Interesting, MTX/UCN-01 eliminated sinusoidal-type metastasis, and only a limited number of portal-type metastases were observed after treatment (Figure 6C). These data were also confirmed by a real-time PCR analysis designed to detect melanoma-specific tyrosinase in mouse livers (Figure 6D).

Discussion

Here, we demonstrated that MyoVa plays a key role in the resistance of melanoma to MTX, indicating that the targeting of this protein in the presence of MTX may prevent drug exportation. However, although direct MyoVa inhibition may be a conceptually attractive strategy for melanoma therapy, its lack of a ligand-binding pocket or measurable catalytic activity makes it a challenging drug target. Therefore, we identified the signaling pathways converging during the MTX-induced activation of MyoVa to design drug-based therapies that will indirectly target this protein in melanoma. In general, the data provided in this study indicate a close homology between two vesicular transport processes: the MTX-induced exportation of melanosomes in melanoma cells and insulin-stimulated GLUT4 membrane translocation in adipocytes. In both processes, the Akt2-dependent phosphorylation of MyoVa appears to be the trigger for vesicle cargo trafficking [23,31]. Together with Akt2, protein kinase Cλ (PKCλ), another phosphoinositol 3-kinase (PI3K)–dependent serine/threonine kinase, has been found to be necessary for insulin-induced glucose transport and GLUT4 translocation [32]. It is well known that insulin simultaneously stimulates the PKCλ/KIF3 and Akt/MyoVa pathways throughout the activation of the PI3K arm; however, how MTX simultaneously activates these molecular pathways is unknown. Interestingly, it has been recently observed that PP2A works as a negative regulator of the insulin metabolic signaling pathway by promoting the dephosphorylation and inactivation of Akt and PKCλ [33]. Therefore, the observation that MTX inhibited PP2A activity by inhibiting the methylation of its catalytic subunit appears to indicate that PP2A inactivation may be a part of its mechanism of action (Figure 7).

In mammals, the Akt protein signaling kinase has been implicated in the regulation of widely divergent cellular processes, such as metabolism, differentiation, proliferation, and apoptosis. Activation of Akt is known to protect against apoptosis induced by a number of stimuli [8,34,35], and several proapoptotic proteins, such as the BH3-only protein Bad, forkhead transcription factors, and caspase-9, have been
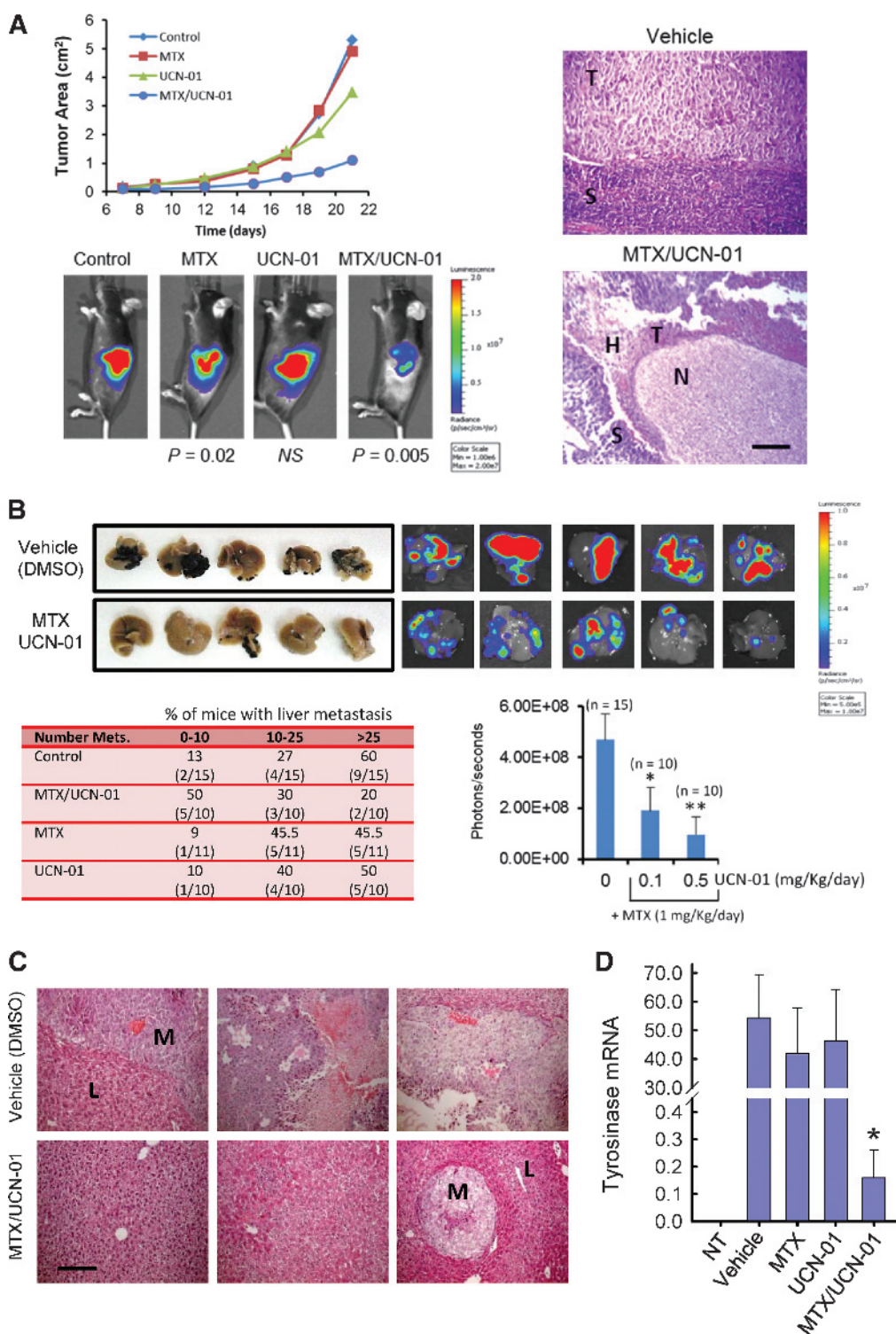
Figure 6. MTX and UCN-01 combination therapy is effective *in vivo*. (A) Treatment: 1 and 0.5 mg/kg per day for MTX and UCN-01, respectively. Left upper panel: B16/F10 cells were subcutaneously injected into C57BL/6 mice. Means are representative of three independent experiments. Differences after 21 days of MTX/UCN-01 treatments were statistically significant ($P < .002$) with respect to control mice or those subjected to individual MTX and UCN-01 treatments. Left lower panel: Representative luciferase imaging of the control and MTX/UCN-01–treated mice 12 days after the intrasplenic injection of tumor cells. NS, not significant. Right panel: Effect of MTX/UCN-01 on B16/F10 primary splenic tumors. Xenograft tumors treated (14 days) with DMSO (vehicle) or MTX/UCN-01. Vehicle-treated tumors showed normal splenic tissue (S) and tumor areas (T) but no discernible necrosis (N). MTX/UCN-01–treated tumors showed hemorrhagic (H) necrosis. Scale bar, 40 μm. (B) Bioluminescent liver imaging 14 days after the intrasplenic injection of B16-F10-luc2 cells from untreated and MTX/UCN-01–treated mice. (C) Photomicrograph (three individuals) of hematoxylin and eosin–stained liver sections from vehicle and MTX/UCN-01–treated mice (5×). Scale bar, 40 μm. (D) Histograms represent the copies of tyrosinase mRNA for every 1 × 10^3 copies of β-actin ± SD. *$P = .001$ between MTX/UCN-01–treated mice and untreated controls (vehicle). Livers form non-melanoma cell inoculated mice (NT) were used as a control.
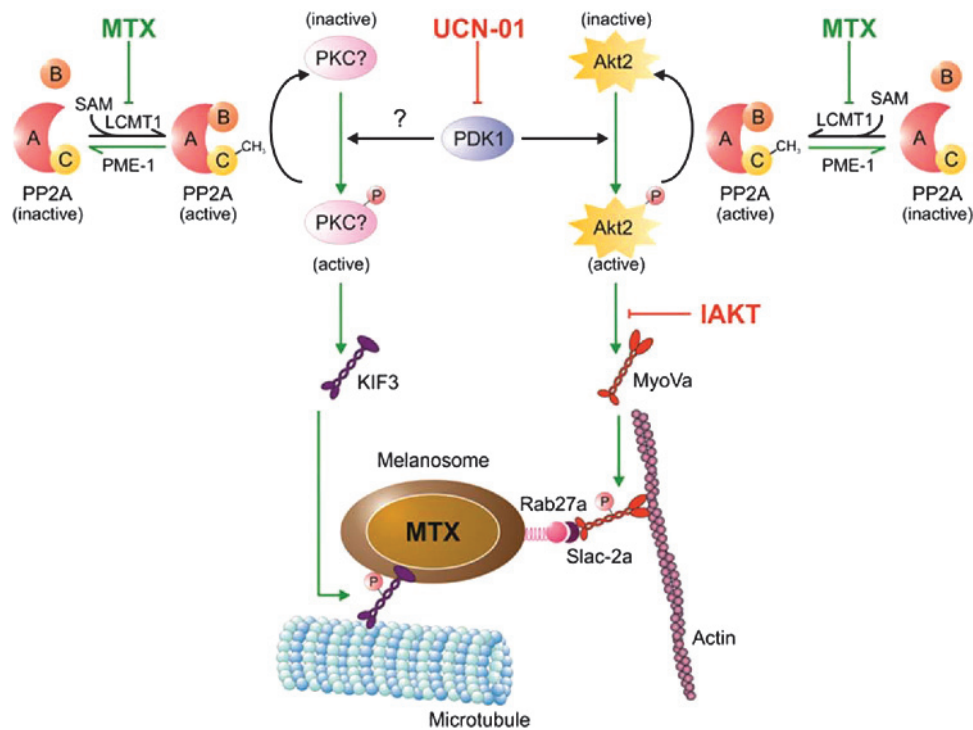
Figure 7. Proposed mechanism for MTX-induced melanosome transport in melanoma. PP2A is a trimeric serine/threonine phosphatase that contains the regulatory subunit B, which is recruited by a C-A dimer composed of the catalytic subunit C (PP2AC) and structural subunit A. Recruitment occurs when C is carboxyl-methylated on the terminal Leu^{309}, resulting in the assembly of the active PP2A trimer. Reversible PP2A methylation is catalyzed by two conserved PP2A-specific enzymes: leucine carboxyl methyltransferase (LCMT-1) and PP2A methylesterase (PME-1). Because LCMT1 is a specific S-adenosyl-L-methionine (SAM)-dependent methyltransferase, the treatment of melanoma cells with MTX may result in the inhibition of the PP2A assembly. The left branch, corresponding with KIF3 activation, is hypothetical and inspired by the insulin-stimulated GLUT4 vesicle translocation process. If an atypical PKC does activate KIF3 in melanoma, UCN-01 treatment would result in the disruption of MTX-stimulated microtubule and actin-dependent melanosome transport because PDK1 is positioned upstream of the Akt and PKC pathways [46]. Green arrows represent MTX-activated pathways, whereas red lines indicate the site of action for the assayed drugs UCN-01 and IAKT.

identified as direct targets that mediate this protective response [8]. Concretely, in melanoma, the Akt3 protein but not Akt1 or Akt2 was increased in melanoma cell lines compared with normal melanocytes [36]. Therefore, although the PTEN/Akt3 signaling cascade has long been recognized as a therapeutic target in melanoma that contributes to the melanoma resistance to chemotherapy [36], the identification of MyoVa as a novel Akt2 proapoptotic target in melanoma might be of general interest. Akt2-mediated MyoVa activation, discovered here as a consequence of MTX action, may represent a general drug resistance mechanism of melanoma cells in response to Akt-activating chemotherapeutic agents [4,6–8] and/or in melanoma with preexisting high, endogenously upregulated, Akt2 activity. It is well known that ER stress leads to Akt activation [37], and recently, the adaptation of melanoma cells to ER stress has been proposed as a resistance mechanism of these cells to chemotherapeutic drugs [8]. Interestingly, melanoma cells are highly resistant to ER stress–inducing drugs such as cisplatin and adriamycin [7,8] but also to drugs that did not cause ER stress such as docetaxel and vincristine, two microtubule-targeting drugs [8]. In the latter case, it was also reported that human melanomas under ER stress were more resistant to apoptosis induced by these drugs due, at least in part, to the activation of the PI3K/Akt pathway. Therefore our results, showing the molecular link between the Akt signaling pathway and the cellular export of chemotherapeutic drugs, might offer a global explanation for multidrug resistance in

melanoma and might be useful to open new avenues for exploring therapeutical combinations of Akt2 inhibitors with MTX or other cytotoxic drugs.

Another attractive possibility to suppress this multidrug resistance mechanism in melanoma might be the inhibition of the PDK1 pathway (Figure 7). Interestingly, UCN-01 decreased insulin-stimulated glucose transport by inhibition of Akt Thr^{308} phosphorylation in isolated rat adipose cells [38]. However, although we precisely demonstrated that UCN-01 inhibited the MTX-induced activation of MyoVa and prevented MTX export in melanoma cells, we cannot exclude that UCN-01–dependent inhibition of other cellular kinases, such as Chk1, might also contribute to the high degree of synergy observed between both drugs in *in vitro* and *in vivo* melanoma models [39]. In fact, this checkpoint kinase has been shown to protect melanomas from MTX-induced apoptosis [9]. Because of the potential for entering the clinical arena, MTX/UCN01 combination, irrespective of the precise action mechanism, must be taken into consideration in the future design of melanoma therapies. MTX is in widespread clinical use for a variety of steroid-recalcitrant inflammatory diseases, and UCN-01 has been included in multiple clinical trial regimes [40,41]; thus, MTX/UCN-01 therapy has the potential for rapid application in the human setting.

It is well known that the amino acid sequence encoded by an alternatively spliced exon, exon F, is necessary for the selective binding of MyoVa to melanosomes [22,42]. The MyoVa isoforms lacking this

amino acid sequence are not targeted to the melanosomes but localized to the perinuclear region instead [22,42]. Although all the melanoma cell lines used in this study presented observable levels of MyoVa exon F expression (Figure W2A), determination of the levels of this MyoVa spliced variant in melanoma biopsy samples could be of interest from a clinical point of view. On the basis of the data obtained in this study, MyoVa could be considered as an oncogenic protein that promotes melanoma resistance to anticancer drugs; therefore, determination of MyoVa exon F in clinical samples of melanoma patients could help in the design of personalized therapies. Although combined therapies to target the Akt2/MyoVa pathway would be functional in melanoma cells having an operative melanosome trafficking system, melanomas showing low or no expression of MyoVa exon F, or related trafficking protein, would not be a clinical problem, because these melanomas would be sensible to classic monotherapy treatments. Therefore, oncologists could decide the most appropriate treatment of melanoma patients in function of MyoVa exon F expression levels in biopsy samples.

In addition to the promising clinical and therapeutic perspectives of these findings, our results may also have implications for understanding the mechanism of action of antifolates in melanoma and identifying the functionality of the proapoptotic pathways in these cancer cells. Although E2F1 has been identified as a component of pathways that link the DNA damage response to cancer cell death [43], this signaling pathway has been barely explored for melanoma therapy. Here, we report that the E2F1 apoptotic pathway is functional in melanoma and that its induction activates p73 and Apaf1 following a p53-autonomous proapoptotic signaling event. In addition, melanoma is often driven by mutations that activate mitogen-activated protein kinase (MAPK) signaling, such as BRAF [27,44]; therefore, the observation that targeting Akt2/MyoVa in the presence of MTX, a compound that blocks essential cell metabolic pathways, induces apoptosis in BRAF-mutated cells may be of potential importance when designing new treatment strategies to improve chemosensitivity, one of the most important obstacles for the management of patients with malignant melanoma.

In conclusion, in this study, we identify a multidrug resistance mechanism that could serve as a link between other resistance mechanisms described in melanoma [4–8]. In this work, the following aspects have been addressed: first, we identified MyoVa as a novel and specific target of Akt2 in melanoma; second, we observed that siRNA or pharmacological blockade of the Akt2/MyoVa pathway in melanoma suppressed MTX resistance in these cancer cells; third, we identified novel druggable targets in this molecular pathway, which could be of interest from a clinical point of view; and fourth, we analyzed the functionality of proapoptotic pathways in melanomas in response to antifolate treatment, by avoiding the cellular export of MTX. Finally, we also observed that the Akt2/MyoVa pathway, similar to insulin-stimulated GLUT4 membrane translocation in adipocytes, is conserved in melanomas. Because this pathway has been extensively characterized in adipocyte cells, the therapy of melanoma can highly benefit from these previous studies.

Acknowledgments

References

[1] American Cancer Society (2011). *Cancer Facts & Figures 2011*. American Cancer Society, Atlanta, GA.

[2] Tawbi HA and Buch SC (2010). Chemotherapy resistance abrogation in metastatic melanoma. *Clin Adv Hematol Oncol* **8**(4), 259–266.

[3] Ascierto PA, Streicher HZ, and Sznol M (2010). Melanoma: a model for testing new agents in combination therapies. *J Transl Med* **8**, 38.

[4] Chen KG, Valencia JC, Lai B, Zhang G, Paterson JK, Rouzaud F, Berens W, Wincovitch SM, Garfield SH, Leapman RD, et al. (2006). Melanosomal sequestration of cytotoxic drugs contributes to the intractability of malignant melanomas. *Proc Natl Acad Sci USA* **103**(26), 9903–9907.

[5] Sánchez-del-Campo L, Montenegro MF, Cabezas-Herrera J, and Rodríguez-López JN (2009). The critical role of alpha-folate receptor in the resistance of melanoma to methotrexate. *Pigment Cell Melanoma Res* **22**(5), 588–600.

[6] Xie T, Nguyen T, Hupe M, and Wei ML (2009). Multidrug resistance decreases with mutations of melanosomal regulatory genes. *Cancer Res* **69**(3), 992–999.

[7] Huang ZM, Chinen M, Chang PJ, Xie T, Zhong L, Demetriou S, Patel MP, Scherzer R, Sviderskaya EV, Bennett DC, et al. (2012). Targeting protein-trafficking pathways alters melanoma treatment sensitivity. *Proc Natl Acad Sci USA* **109**(2), 553–558.

[8] Jiang CC, Yang F, Thorne RF, Zhu BK, Hersey P, and Zhang XD (2009). Human melanoma cells under endoplasmic reticulum stress acquire resistance to microtubule-targeting drugs through XBP-1–mediated activation of Akt. *Neoplasia* **11**(5), 436–447.

[9] Sáez-Ayala M, Fernández-Pérez MP, Montenegro MF, Sánchez-del-Campo L, Chazarra S, Piñero-Madrona A, Cabezas-Herrera J, and Rodríguez-López JN (2012). Melanoma coordinates general and cell-specific mechanisms to promote methotrexate resistance. *Exp Cell Res* **318**(10), 1146–1159.

[10] Mehta AD, Rock RS, Rief M, Spudich JA, Mooseker MS, and Cheney RE (1999). Myosin-V is a processive actin-based motor. *Nature* **400**(6744), 590–593.

[11] Kufe DW, Wick MM, and Abelson HT (1980). Natural resistance to methotrexate in human melanomas. *J Invest Dermatol* **75**(4), 357–359.

[12] Sánchez-del-Campo L and Rodríguez-López JN (2008). Targeting the methionine cycle for melanoma therapy with 3-O-(3,4,5-trimethoxybenzoyl)-(–)-epicatechin. *Int J Cancer* **123**(10), 2446–2455.

[13] Watabe H, Valencia JC, Yasumoto K, Kushimoto T, Ando H, Muller J, Vieira WD, Mizoguchi M, Appella E, and Hearing VJ (2004). Regulation of tyrosinase processing and trafficking by organellar pH and by proteasome activity. *J Biol Chem* **279**(9), 7971–7981.

[14] Potterf SB, Muller J, Bernardini I, Tietze F, Kobayashi T, Hearing VJ, and Gahl WA (1996). Characterization of a melanosomal transport system in murine melanocytes mediating entry of the melanogenic substrate tyrosine. *J Biol Chem* **271**(8), 4002–4008.

[15] Angus SP, Wheeler LJ, Ranmal SA, Zhang X, Markey MP, Mathews CK, and Knudsen ES (2002). Retinoblastoma tumor suppressor targets dNTP metabolism to regulate DNA replication. *J Biol Chem* **277**(46), 44376–44384.

[16] Shevchenko A, Wilm M, Vorm O, and Mann M (1996). Mass spectrometric sequencing of proteins silver-stained polyacrylamide gels. *Anal Chem* **68**(46), 850–858.

[17] Vidal-Vanaclocha F, Amezaga C, Asumendi A, Kaplanski G, and Dinarello CA (1994). Interleukin-1 receptor blockade reduces the number and size of murine B16 melanoma hepatic metastases. *Cancer Res* **154**(10), 2667–2672.

[18] Hirokawa N and Noda Y (2008). Intracellular transport and kinesin superfamily proteins, KIFs: structure, function, and dynamics. *Physiol Rev* **88**(3), 1089–1118.

[19] Armstrong JM, Krementsova E, Michalek AJ, Heaslip AT, Nelson SR, Trybus KM, and Warshaw DM (2012). Full-length myosin Va exhibits altered gating during processive movement on actin. *Proc Natl Acad Sci USA* **109**(5), E218–E224.

[20] Wu X, Wang F, Rao K, Sellers JR, and Hammer JA III (2002). Rab27a is an essential component of melanosome receptor for myosin Va. *Mol Biol Cell* **13**(5), 1735–1749.

[21] Strom M, Hume AN, Tarafder AK, Barkagianni E, and Seabra MC (2002). A family of Rab27-binding proteins. Melanophilin links Rab27a and myosin Va function in melanosome transport. *J Biol Chem* **277**(28), 25423–25430.

[22] Van Gele M, Geusens B, Schmitt AM, Aguilar L, and Lambert J (2008). Knockdown of myosin Va isoforms by RNAi as a tool to block melanosome transport in primary human melanocytes. *J Invest Dermatol* **128**(10), 2474–2484.

[23] Yoshizaki T, Imamura T, Babendure JL, Lu JC, Sonoda N, and Olefsky JM (2007). Myosin 5a is an insulin-stimulated Akt2 (protein kinase Bβ) substrate modulating GLUT4 vesicle translocation. *Mol Cell Biol* **27**(14), 5172–5183.

[24] Winter-Vann AM, Kamen BA, Bergo MO, Young SG, Melnyk S, James SJ, and Casey PJ (2003). Targeting Ras signaling through inhibition of carboxyl methylation: an unexpected property of methotrexate. *Proc Natl Acad Sci USA* **100**(11), 6529–6534.

[25] Andrabi S, Gjoerup OV, Kean JA, Roberts TM, and Schaffhausen B (2007). Protein phosphatase 2A regulates life and death decisions via Akt in a context-dependent manner. *Proc Natl Acad Sci USA* **104**(48), 19011–19016.

[26] Sato S, Fujita N, and Tsuruo T (2007). Interference with PDK1-Akt survival signaling pathway by UCN-01 (7-hydroxystaurosporine). *Oncogene* **21**(11), 1727–1738.

[27] Fecher LA, Cummings SD, Keefe MJ, and Alani RM (2007). Toward a molecular classification of melanoma. *J Clin Oncol* **25**(12), 1606–1620.

[28] Wang A, Li CJ, Reddy PV, and Pardee AB (2005). Cancer chemotherapy by deoxynucleotide depletion and E2F-1 elevation. *Cancer Res* **65**(17), 7809–7814.

[29] Sedelnikova OA, Pilch DR, Redon C, and Bonner WM (2003). Histone H2AX in DNA damage and repair. *Cancer Biol Ther* **2**(3), 233–235.

[30] Korotayev K and Ginsberg D (2008). Many pathways to apoptosis: E2F1 regulates splicing of apoptotic genes. *Cell Death Differ* **15**(12), 1813–1814.

[31] Guo HL, Zhang C, Liu Q, Li Q, Lian G, Wu D, Li X, Zhang W, Shen Y, Ye Z, et al. (2012). The Axin/TNKS complex interacts with KIF3A and is required for insulin-stimulated GLUT4 translocation. *Cell Res* **22**(8), 1246–1257.

[32] Imamura T, Huang J, Usui I, Satoh H, Bever J, and Olefsky JM (2003). Insulin-induced GLUT4 translocation involves protein kinase C-λ-mediated functional coupling between Rab4 and the motor protein kinesin. *Mol Cell Biol* **23**(14), 4892–4900.

[33] Ugi S, Imamura T, Maegawa H, Egawa K, Yoshizaki T, Shi K, Obata T, Ebina Y, Kashiwagi A, and Olefsky JM (2004). Protein phosphatase 2A negatively regulates insulin's metabolic signaling pathway by inhibiting Akt (protein kinase B) activity in 3T3-L1 adipocytes. *Mol Cell Biol* **24**(19), 8778–8789.

[34] Hollander MC, Balogh AR, Liwanag J, Han W, Linnoila RI, Anver MR, and Dennis PA (2008). Strain-specific spontaneous and NNK-mediated tumorigenesis in *Pten+/–* mice. *Neoplasia* **10**(8), 866–872.

[35] Dummler B, Tschopp O, Hynx D, Yang ZZ, Dirnhofer S, and Hemmings BA (2006). Life with a single isoform of Akt: mice lacking Akt2 and Akt3 are viable but display impaired glucose homeostasis and growth deficiencies. *Mol Cell Biol* **26**(21), 8042–8051.

[36] Stahl JM, Sharma A, Cheung M, Zimmerman M, Cheng JQ, Bosenberg MW, Kester M, Sandirasegarane L, and Robertson GP (2004). Deregulated Akt3

[37] Hu P, Han Z, Couvillon AD, and Exton JH (2004). Critical role of endogenous Akt/IAPs and MEK1/ERK pathways in counteracting endoplasmic reticulum stress-induced cell death. *J Biol Chem* **279**(47), 49420–49429.

[38] Kondapaka SB, Zarnowski M, Yver DR, Sausville EA, and Cushman SW (2004). 7-hydroxystaurosporine (UCN-01) inhibition of Akt Thr^{308} but not Ser^{473} phosphorylation: a basis for decreased insulin-stimulated glucose transport. *Clin Cancer Res* **10**(21), 7192–7198.

[39] Sampath D, Shi Z, and Plunkett W (2002). Inhibition of cyclin-dependent kinase 2 by the Chk1-Cdc25A pathway during the S-phase checkpoint activated by fludarabine: dysregulation by 7-hydroxystaurosporine. *Mol Pharmacol* **62**(3), 680–688.

[40] Dees EC, Baker SD, O'Reilly S, Rudek MA, Davidson SB, Aylesworth C, Elza-Brown K, Carducci MA, and Donehower RC (2005). A phase I and pharmacokinetic study of short infusions of UCN-01 in patients with refractory solid tumors. *Clin Cancer Res* **11**(2), 664–671.

[41] Schenk EL, Koh BD, Flatten KS, Peterson KL, Parry D, Hess AD, Smith BD, Karp JE, Karnitz LM, and Kaufmann SH (2012). Effects of selective checkpoint kinase 1 inhibition on cytarabine cytotoxicity in acute myelogenous leukemia cells *in vitro*. *Clin Cancer Res* **18**(19), 5364–5373.

[42] Au JS and Huang JD (2002). A tissue-specific exon of myosin Va is responsible for selective cargo binding in melanocytes. *Cell Motil Cytoskeleton* **53**(2), 89–102.

[43] Engelmann D, Knoll S, Ewerth D, Steder M, Stoll A, and Pützer BM (2010). Functional interplay between E2F1 and chemotherapeutic drugs defines immediate E2F1 target genes crucial for cancer cell death. *Cell Mol Life Sci* **67**(6), 931–948.

[44] Tap WD, Gong KW, Dering J, Tseng Y, Ginther C, Pauletti G, Glaspy JA, Essner R, Bollag G, Hirth P, et al. (2010). Pharmacodynamic characterization of the efficacy signals due to selective BRAF inhibition with PLX4032 in malignant melanoma. *Neoplasia* **12**(8), 637–649.

[45] Cokol M, Chua HN, Tasan M, Mutlu B, Weinstein ZB, Suzuki Y, Nergiz ME, Costanzo M, Baryshnikova A, Giaever G, et al. (2011). Systematic exploration of synergistic drug pairs. *Mol Syst Biol* **7**, 544.

[46] Hodgkinson CP and Sale GJ (2002). Regulation of both PDK1 and the phosphorylation of PKC-ζ and -δ by a C-terminal PRK2 fragment. *Biochemistry* **41**(2), 561–569.
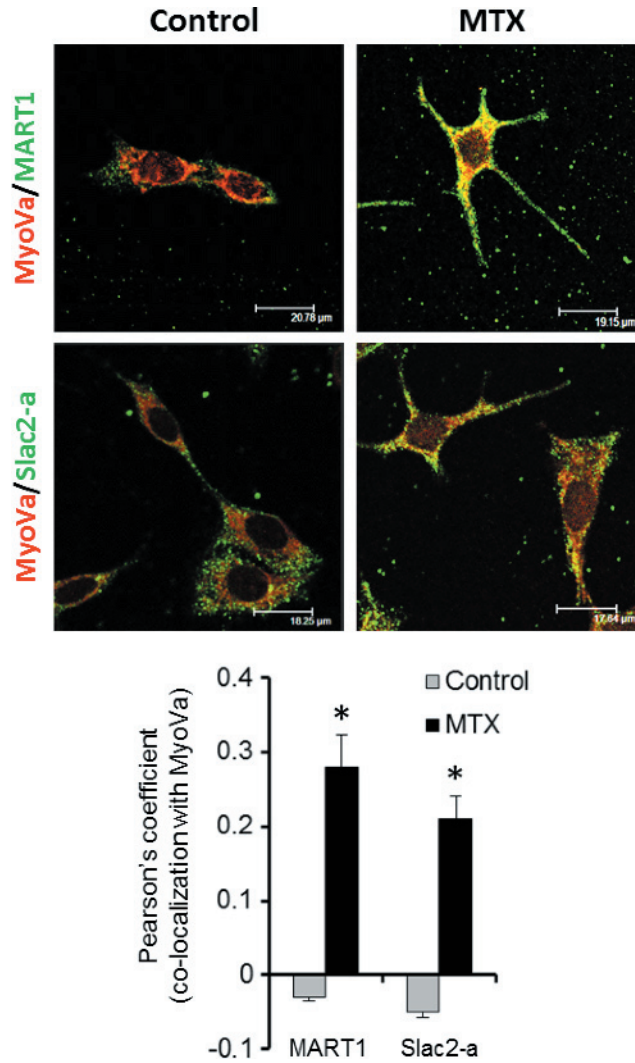
Figure W1. IHC was performed to analyze the localization of MyoVa in untreated B16/F10 melanoma cells and in cells treated for 4 hours with 1 μM MTX. Confocal images represent merged images of the localization of MyoVa with Melan-A/MART1 (melanosome marker) and Slac2-a. From the confocal images, a Pearson coefficient was calculated to estimate the degree of co-localization of Melan-A/ MART1 and Slac2-a with MyoVa (histograms). The Pearson overlap coefficients are represented as the average of 10 individual cells. *$P < .05$ with respect to untreated control cells.
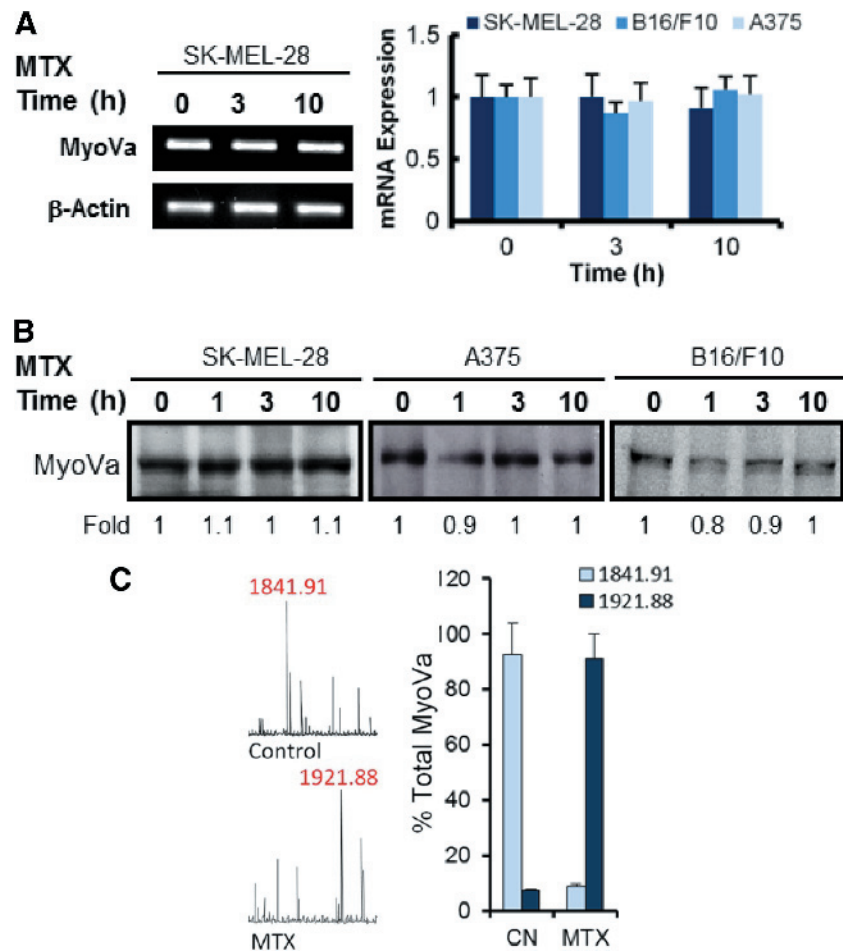
Figure W2. MTX leads to MyoVa phosphorylation in melanoma. (A) The effect of MTX (1 μM) on MyoVa–exon F mRNA expression was assayed by conventional PCR (left panel) and quantitative real-time PCR (right panel). The estimated levels of mRNA relative to β-actin mRNA in MTX-treated cells were calculated and compared with the expression levels in untreated cells (one-fold). The differences between the treated cells and their respective untreated controls were not significant. (B) The effect of MTX treatment (1 μM) on MyoVa protein levels in different melanoma cell lines was assayed by WB using an antibody designed to detect all known MyoVa splice variants. The MyoVa protein levels were normalized to the β-actin protein levels and their respective controls (one-fold). (C) MALDI-TOF mass spectra of phosphorylated and non-phosphorylated peptides (at Ser[1650]) in MyoVa–trypsin-digested samples (Table W1). Peptides were analyzed in untreated SK-MEL-28 (control) or treated (10 hours) with 1 μM MTX.

**Table W1.** MALDI-TOF Spectroscopy Properties of Immunoprecipitated MyoVa Tryptic Digests.

Modification	MyoVa Status	Peptide Sequence*	Measured (*m/z*)	Theoretical (*m/z*)	Control[†] (Intensity)[‡]	MTX[†] (Intensity)[‡]
Phosphorylation (S1650)	Non-phosphorylated	(R)TSSIADEGTYTLDSILR(Q)	1,841.91	1,841.99	101,324	9,512
	Phosphorylated	(R)TSpSIADEGTYTLDSILR(Q)	1,921.88	1,921.99	7,835	98,451
Phosphorylation (S1812)	Non-phosphorylated	(R)KDSPQLLMDAK(H)	1,245.65	1,245.46	112,843	10,514
	Phosphorylated	(R)KDSpPQLLMDAK(H)	1,325.25	1,325.46	2,305	2,525

*The characteristic peptides involving phosphorylation of MyoVa (phosphorylation, P), as well as their measured and theoretical *m/z*, are shown.
[†]Peptides were analyzed in untreated SK-MEL-28 cells (control) and those treated with 1 µM MTX for 10 hours.
[‡]Relative intensities of specific tryptic peptides were normalized with respect to an internal matrix control.
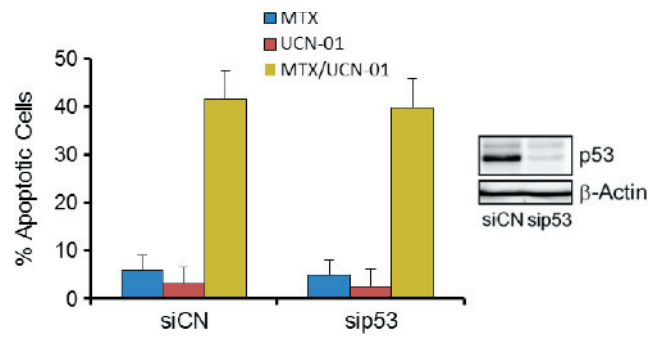
Figure W3. The effect of p53 silencing on MTX/UCN-01–induced apoptosis in G361 (p53 wild-type) melanoma cells. MTX (1 μM) and/or UCN-01 (50 nM) was added to the indicated G361 melanoma cells, and apoptosis was determined after 3 days. p53 was silenced in G361 cells as indicated and shown in a WB (inset).